

Free-Free Spectral Energy Distributions of Hierarchically Clumped H II Regions

Richard Ignace¹ & Ed Churchwell

Department of Astronomy, University of Wisconsin, 5534 Sterling Hall, 475 N. Charter St., Madison, WI 53706-1582

A B S T R A C T

In an effort to understand unusual power-law spectral slopes observed in some hypercompact H II regions, we consider the radio continuum energy distribution from an ensemble of spherical clumps. An analytic expression for the free-free emission from a single spherical clump is derived. The radio continuum slope (with $F_\nu \propto \nu^{-\alpha}$) is governed by the population of clump optical depths τ_ν , such that (a) at frequencies where all clumps are thick, a continuum slope of +2 is found, (b) at frequencies where all clumps are optically thin, a flattened slope of 0:11 is found, and (c) at intermediate frequencies, a power-law segment of significant bandwidth with slopes between these two limiting values can result. For the ensemble distribution, we adopt a power-law distribution $N(\tau) \propto \tau^{-\beta}$, and find that significant power-law segments in the SED with slopes from +2 to 0:11 result only for a relatively restricted range of values of β of 1 to 2. Further, a greater range of clump optical depths for this distribution leads to a wider bandwidth over which the intermediate power-law segment exists. The model is applied to the source W 49N-B2 with an observed slope of $\alpha = +0.9$, but that may be turning over to become optically thin around 2 mm. An adequate fit is found in which most clumps are optically thin and there is little "shadowing" of rearward clumps by foreground clumps (i.e., the geometrical covering factor $C < 1$). The primary insight gained from our study is that in the Rayleigh-Jeans limit for the Planck function that applies for the radio band, it is the distribution in optical depth of the clump population that is solely responsible for setting the continuum shape, with variations in the size and temperature of clumps serving to modulate the level of free-free emission.

Subject headings: Radiative Transfer { Stars: Circumstellar Matter { Stars: Formation { ISM : H II Regions { Radio Continuum : Stars

1. INTRODUCTION

During the past few years a new class of super-compact H II regions has been recognized via high resolution radio observations. This class of objects is now referred to as hypercompact (HC) H II regions (Gaume 1994; Kurtz 2000). HC H II regions are typically about ten times smaller and about a hundred times denser than ultracompact (UC) H II regions (Kurtz and Franco 2000; Kurtz 2002) and have emission measures typically 10^8 pc cm^{-6} . HC H II regions also have rising spectral energy distributions (SEDs) from short cm to mm wavelengths (Hofner et al. 1996; Kurtz 2002; Sewilo et al. 2003 and references therein) and often have unusually broad radio recombination lines ($\sim 40 \text{ km s}^{-1}$) (Gaume 1994; Gaume et al. 1995; Shepherd et al. 1995; DePree, Mehlinger, & Goss 1997; Sewilo et al. 2003). Some HC H II regions (see Sewilo et al. 2003), like some UC H II regions (see Koo et al. 1996; Garay et al. 1993; and Kurtz et al. 1999) are surrounded by extended low-density ionized halos. The most likely explanation for the halos is that HC and UC H II regions are highly clumped, thereby producing porous nebulae to UV photons. An example of

¹Currently at Department of Physics and Astronomy, East Tennessee State University; Email: ignace@mail.etsu.edu

a HC H II region with a power-law SED is G 75.78+ 0.34-H₂O, whose spectrum from 6 cm to 7 mm is shown in Figure 1.

HC H II regions are found in the vicinity of massive star formation and are often coincident with strong H₂O masers. Some HC H II regions appear to be driving bipolar molecular outflows (Hofner et al. 1996; Shepherd et al. 1998). Sewilo et al. (2003) have suggested that HC H II regions may represent an evolutionary stage between hot molecular cores and UC H II regions. During this period, rapid accretion onto the central protostar shuts down, and a circumstellar H II region first becomes large enough to be detected. A property of at least some HC H II regions that concerns this paper is their power-law SEDs at radio wavelengths. The SEDs of HC H II regions have spectral indices between +0.3 to +1.6 (S/ν^2) with typical values of $\alpha + 1$ from short cm to mm wavelengths. All HC H II regions seem to have rising power spectra in the range 3.6 cm to 3 mm, but the slopes may differ from source to source.

These spectral indices are especially interesting because they cannot easily be explained by thermal or nonthermal radio continuum emission for constant density nebulae. They are too shallow for optically thick thermal emission, too steep for optically thin thermal emission, and the wavelength interval is too broad to represent the transition from optically thick to thin thermal emission. The spectral indices are inconsistent with optically thin synchrotron emission; also, radio recombination lines require that HC H II regions are thermal. In this paper, we explore the possibility that the power-law SEDs of HC H II regions might possibly be the result of hierarchical clumping.

It has been known for some time that power-law density gradients with distance from the ionizing star of H II regions produce radio power-law SEDs (O'lon 1975; Panagia & Felli 1975; Wright & Barlow 1975). O'lon (1975) showed that the relationship between the slope of the SED (α) and the slope of the power-law density gradient (n_e/r^{β} where n_e is density) is $\alpha = (\beta - 3)/2 = (\beta - 0.5)/1$ for $\beta > 1.5$. Thus, for $\alpha = 0.6$, $\beta = 2.0$; for $\alpha = +1$, $\beta = 2.6$; and for $\alpha = +1.5$, $\beta = 4.7$. The $\alpha = 0.6$, $\beta = 2.0$ parameters correspond to the classical values for a constant velocity wind (Wright & Barlow 1975; Panagia & Felli 1975). O'lon (1975) points out that when the density gradient has a power-law dependence on radius, the slope of the SED will be determined by the value of β at the radius where the optical depth is about unity. That is, the size of the effective radiating surface depends on both the density gradient and frequency. Hartmann & Cassinelli (1977) showed that a radial outflow whose velocity is a power-law with radius of index β has a density power-law dependence on radius of $\beta - 2$, resulting in a SED power-law ($S/\nu^{2-\beta}$ for a constant velocity wind). The density power-law index β increases so rapidly with β that β is improbably large for $\alpha + 1$ ($\beta = 2.6$). In light of the observed density structure of H II regions discussed above, it seems unlikely that real H II regions have such steep and well-behaved density structures with radius, especially in the very early stages of evolution expected for HC H II regions. We therefore investigate an alternate possible explanation for the observed radio power-law SEDs of HC H II regions, namely hierarchical clumping of nebular gas.

As used here, "hierarchical clumping" refers to a region filled with clumps of ionized gas having a range of sizes, temperatures, and optical depths defined by power-law distributions. There need not be a medium in which all the clumps are embedded although such a structure could be accommodated in our analysis. A hierarchical clump distribution is not the same as a fractal distribution which posits clumps within clumps within clumps. In a fractal structure the emergent SED is complicated by the fact that every clump is embedded in clumps of larger size, whereas in a hierarchically clumped structure the main complication arises when clumps begin to shadow other clumps, otherwise one does not have to be concerned with radiation transfer through a myriad of larger clumps.

The fact that the interstellar medium (ISM) seems to be clumped on all observed size scales in H II regions, planetary nebulae, and neutral atomic and molecular clouds is a strong motivation for the study presented here. High resolution Hubble Space Telescope (HST) images of the Orion nebula (O'Dell 2001 and references therein) have revealed an array of small-scale, ionized structures down to the resolution limit of the HST. The small-scale structures (clumps, filaments, knots, etc) are easiest to recognize in Orion because

of its proximity to us, but high resolution observations of other H II regions such as M 16 also indicate that they are composed of a complex of many clumps of varying sizes (Hester et al. 1996). It is unlikely that the clumpy structures in Orion and M 16 are unique; rather, they probably indicate that such structure is inherent in all H II regions. Small scale ionized clumps are also seen in planetary nebulae (O'Dell et al. 2002, 2003). High resolution V L B I observations of Galactic H I absorption toward quasars (Faison & Goss 2001; Faison et al. 1998) show that very small clumps (on the order of a few AU) exist in neutral Galactic H I clouds. Extensive CO observations (e.g., Falgarone & Phillips 1996; Elmegreen & Falgarone 1996; Falgarone et al. 1998) have clearly demonstrated the existence of small-scale structures in molecular clouds.

The origin of the clumpy structure in the various phases of the ISM is controversial and may have different explanations in different environments. For example, turbulence has been suggested by several authors as the origin of structure in molecular and H I clouds (Elmegreen & Falgarone 1996; Falgarone et al. 1998; Lazarian & Pogosyan 2000). However, at least some of the structure in H II regions may be due to hydrodynamical instabilities and/or to pre-existing structure in the natal cloud of an emerging H C H II region. The reason for clumpy structures in the ISM around massive stars is beyond the scope of this paper. Here, the observationally established clumpiness of the ISM plus the presence of extended halos around U C and H C H II regions motivates our analysis of the radio free-free spectra of hierarchically clumpy H C H II regions.

In the following section, we derive an analytic expression for the free-free emission from a single spherical clump, and employ the result to consider the radio SEDs from an ensemble of clumps. In §3, the model is applied to the source W 49N-B2. A brief discussion of the model and its results appear in §4, and concluding remarks given in §5.

2. FREE-FREE EMISSION FROM SPHERICAL CLUMPS

2.1. Emission from a Single Clump

Let us begin our discussion by examining the spectrum of a single spherical clump of uniform density, temperature, and ionization. A closely related problem has been solved by Osterbrock (1974). Here the result is expressed in a slightly different form in order to determine the unresolved flux of emission from an ensemble of clumps.

We begin with a discussion of the total optical depth along any ray that passes through a clump. Its value is given by

$$\tau(p) = 2 \int_0^R \kappa(p; T) z(p); \quad (1)$$

where κ is the opacity, ρ the clump density, T the clump temperature, p the impact parameter of the ray, and $z = \frac{2R}{\sqrt{R^2 - p^2}}$ the total length of the ray through the clump, with R being the clump radius. If we may further assume a constant source function S for the clump emission, then the emergent intensity I from the clump along this ray is

$$I = S \int_0^{\tau(p)} e^{-\tau} d\tau; \quad (2)$$

Correspondingly, the total flux emitted by an unresolved clump will be given by

$$F = \frac{2}{D^2} S \int_0^R \int_0^{\sqrt{R^2 - p^2}} e^{-\tau(p)} p dp \quad (3)$$

Through a change of variable, whereby the integral is evaluated in z instead of p , the preceding expression can be solved to obtain

$$F = \frac{2 R^2}{D^2} S \int_0^1 \frac{2}{t^2} (1+t) e^{-t} dt; \quad (4)$$

where

$$t = 2 \tau (R) R; \quad (5)$$

is the optical depth along the clump's diameter. Equation (4) has the correct limits, in that for a very thick clump with $t \gg 1$, the flux depends on the source function and clump cross-section with $F \approx S R^2 = D^2$, and for a thin clump with $t \ll 1$, the flux expression reduces to $2 t S R^2 = 3 D^2$. Substituting in for t , one finds that optically thin clumps have a flux given by the product of the clump volume and the emissivity, as expected.

For the case at hand, we shall consider only free-free emission at long wavelengths appropriate for the radio band. The source function will be Planckian, with $S = B = 2kT \frac{2}{c^2}$, and the product of opacity and density will be given by

$$\tau (R; T) = 0.018 Z_i^2 T^{3/2} g_{ff}^2 \frac{1}{n_i n_e m_H^2} \text{ cm}^{-1}; \quad (6)$$

where Z_i is the ion charge, g_{ff} ($= 1 \text{ GHz}$)^{0.11} is the Gaunt factor, n_i and n_e are the ion and electron mean molecular weights, m_H is the mass of hydrogen, T is in K, R is in Hz, and ρ is in g cm^{-3} . Equation (6) is based on an expression appearing in x5.9 of Allen's Astrophysical Quantities (4th ed., Cox 2000).

2.2. Emission from a Distribution of Clumps

In considering the free-free emission from an ensemble of clumps, it is necessary first to make a few remarks about the emission from a single clump as given in equation (4) and expressions following. First, the basic variables for the emission include R , T , ρ , t , and τ , but these are not independent. In particular, t depends on all 4 of the other variables. Moreover, density is the only variable that does not appear explicitly in the flux equation.

We choose to ignore density in the discussion to follow and consider the flux to be a function of R , T , t , and τ . Moreover, our discussion concerns free-free emission in the radio band, and already, it has been noted that we shall assume the Rayleigh-Jeans limit for B , the source function. Folding these assumptions into equation (4), we have that

$$F = \frac{4 k T R^2}{c^2 D^2} G(t); \quad (7)$$

where

$$G(t) = \int_0^1 \frac{2}{t^2} (1+t) e^{-t} dt; \quad (8)$$

We thus come to a remarkable conclusion. In the treatment at hand, ν is a spectral variable. A distribution of clumps will thus depend on R , T , and t , but it is only t that depends on frequency. This means that

if R , T , and t can be treated as independent variables for describing the distribution of emitting clumps, it is only the distribution in t that can affect the spectral shape, whereas the distributions in R and T can influence only the flux scale. Consequently, we shall not consider distributions in R and T and replace their appearance with average quantities. For example with a distribution of N_{cl} clumps at fixed diameter optical depth t (allowing for different temperatures, sizes, and densities), equation (7) would become

$$F = \frac{4}{c^2 D^2} \frac{k T_i h R^2 i}{f^2} N_{cl} f^2 G(t); \tag{9}$$

where we have introduced a normalized frequency $f = \nu / \nu_0$ with ν_0 a fiducial value.

In Figure 2, a plot of G versus t is shown. At small optical depth, $G \propto t$, whereas at high optical depth, the function is given by $G \propto t^{-1}$. This figure shows how clumps of different optical depths will contribute in a large ensemble. However, noting that $t \propto f^{-2} g \propto f^{-2.11}$, Figure 2 also suggests how a single clump contributes to the ensemble total at different frequencies. From this perspective low t corresponds to high f , and vice versa. The implication is that for any given clump, there will always be frequencies at which the clump is thin and frequencies where it is thick.

Thus equation (7) is found to have two important limits. For clumps that are very thick (i.e., $t \gg 1$), the resultant SED will be proportional to $f^2 G \propto f^2$. If all the clumps are thin, then the SED will approach $f^2 G \propto f^{0.11}$ which is the scaling for the Gaunt factor in the radio band. The variation between thick and thin thus gives a power-law range between -0.11 and $+2$, so that in principle, one can imagine a frequency "window" over which the SED may approximate a power-law with a slope that is intermediate between these two limiting values. Note that we are ignoring contributions from the central star because the radio continuum emission of the star will be dwarfed by the contribution from the H II region; however, the star and its immediate circumstellar component may start to compete with the extended emission at the shorter mm and far-IR wavelengths.

We now introduce a power-law number distribution in terms of the optical depth along the clump diameter:

$$N(t) = N_0 t^{-\alpha}; \tag{10}$$

such that the total number of clumps N_{cl} is given by

$$N_{cl} = N_0 \int_{t_1}^{t_2} t^{-\alpha} dt; \tag{11}$$

and N_0 is a normalization constant. Now mean physical parameters such as hT_i and $hR^2 i$ are defined with reference to this optical depth distribution. Care must be taken in handling this distribution, since $t = t(f)$. One must ensure that the total number of clumps N_{cl} is the same for all frequencies, requiring that the normalization constant is a function of frequency, which is given by

$$N_0(f) = (1 - \alpha) N_{cl} \frac{1}{t_2^{1-\alpha}} \frac{1}{t_1^{1-\alpha}} / g^{-1} f^{2(1-\alpha)}; \tag{12}$$

Thus the normalization can be a fairly strong function of frequency.

The total flux of emission from the ensemble of unresolved clumps is given by the following integral expression:

$$F_{\text{tot}}(f) = N_{\text{cl}} F_0 f^2 \frac{\int_{t_1}^{R_{t_2}} N(t) G(t) dt}{\int_{t_1}^{R_{t_2}} N(t) dt}; \quad (13)$$

where

$$F_0 = \frac{4 \pi^2 k T_0 h R^2 i}{c^2 D^2}; \quad (14)$$

Expression (13) indicates that the total flux from the distribution of clumps is equivalent to the average flux times the total number of clumps in the volume. Implicit is that there is no shadowing of one clump by another. Our approach does not allow for emission by one clump to be absorbed by another clump and re-processed.

An expression of the shadowing effect can be estimated in terms of a covering factor, C . We define this to be the projected area of all the clumps, divided by the projected area of the volume in which the clumps reside. Suppose that the volume is spherical of radius L , then we have that

$$C = \frac{A_{\text{tot}}}{L^2} = N_{\text{cl}} \frac{h R^2 i}{L^2}; \quad (15)$$

Again, our analysis is only valid if the covering factor is less than unity. It is certainly clear that $h R^2 i = L^2 < 1$ must hold, otherwise one does not really have a distribution of clumps, but a volume-filling cloud.

As an illustration of how C depends on the clump distribution, we assume a power law distribution of sizes given by $N(R) / R^3$, bounded by R_{max} and R_{min} . In Figure 3, we plot the covering factor as a function of f for different values of $R_{\text{max}}^2 = L^2 < 1$ and ratios $R_{\text{min}} = R_{\text{max}}$ as indicated in each panel of the figure. The value of N_{cl} is varied to give the different curves appearing in each panel, with the lowest curve always for $N_{\text{cl}} = 1$, and the highest curve for $N_{\text{cl}} = 10^7$. Although our analysis does not explicitly determine R_{min} , or R_{max} , the application of our method does allow inference of C , that can constrain the parameters that describe the clump size distribution.

2.3. Limits for the Clump Distribution

It is worthwhile to consider the limiting properties of clumps that might influence the model SEDs. One such example is that clumps that are sufficiently massive can collapse under their own self-gravity. This is behavior that we seek to avoid, so we need to estimate its domain. If we take collapse to occur when the self-gravity of the clump exceeds its thermal internal energy, and apply our assumptions of constant density and temperature, then a limit to the density for a given clump radius can be derived. The governing expressions for collapse are

$$\frac{3}{2} N k T_0 - \frac{3 G M^2}{5 R} < 0; \quad (16)$$

where the clump mass is $M = 4 \pi R^3 \rho$, and the number of particles is $N = M / m$, for an average particle mass of m . Rearranging the expression, one finds an upper limit to the clump size for a given density:

$$R < \frac{5}{4} \frac{m}{G \rho}; \quad (17)$$

For a reasonable cold cloud temperature of $T_0 = 30 \text{ K}$, and for a quite large cloud number density of 10^9 cm^{-3} corresponding to a density of $10^{15} \text{ g cm}^{-3}$, the cloud will begin to collapse if its size exceeds a value of about 500 AU. For a radio measurement around 10 GHz, the implied clump optical depth is about 10^6 . However, this density is extreme, and values more typical of dense clouds will be about 3 orders of magnitude smaller. Since $R < 1=2$, the upper limit to the scale of dense clouds mushrooms to about 0.07 pc, with a corresponding optical depth at 10 GHz of nearly 100. But a size of 0.07 pc is comparable to the size (if not larger) of an entire H C H II region. Consequently, the condition of cloud collapse does not provide a significant physical constraint on the distribution of cloud sizes, nor the cloud optical depths.

However, there is another condition that provides a limit to the size and density of the clump. For a clump to contribute to the observed spectrum, it must survive the strong UV photo-ionizing radiation field of the central source, otherwise the clump will have evaporated to merge with the lower density diffuse gas of the region. We estimate this limit as follows. Let n be the total density of the clump, including neutrals n_n and ions n_i . We imagine that the star "turns on", producing an ionization front for every clump. The differential equation governing the relative growth of ions in the clump will involve a competition between the ionizing radiation field of the central star, which we represent with N_{γ} for the number of ionizing photons emitted each second, and the recombination of the gas, which is represented by N_{rec} for the number of recombinations each second.

It is convenient to work with number densities n and particle numbers N for the neutral and ionized gas. The gas is assumed to be pure hydrogen with $n_H = n$. The particle number is related to the number density and volume via $N = nV$, where V is the volume appropriate for the species being considered (i.e., if n refers to the neutral gas, then V is the volume in the clump with neutral hydrogen). We take the evolution of the clump ionization as

$$N_{\dot{i}} = W(R;r)N_{\gamma} - N_{\text{rec}}; \tag{18}$$

where $W(R;r) = R^2=4r^2$ is the geometrical dilution factor (in this case, the solid angle of the clump as seen from the vantage of the central star at distance r from the clump), and hence is the fraction of the ionizing radiation from the central source that impinges on the clump. We further identify

$$N_{\text{rec}} = n_i n_e \text{rec} V_{\text{ioniz}}; \tag{19}$$

where rec is a recombination coefficient in $\text{cm}^3 \text{s}^{-1}$, $n_i = n_e$, and V_{ioniz} references the volume of ionized gas. It is assumed that the total volume of the clump does not change. For simplicity, ionized particles are not allowed to leave the clump, nor do ions and neutrals mix, with the consequence that $n_i = n_H$ in the relevant volumes.

Incorporating these assumptions and definitions, the equation for the clump ionization becomes

$$N_{\dot{i}} = W(R;r)N_{\gamma} - \text{rec} n_H N_i; \tag{20}$$

This is a standard inhomogeneous first order linear differential equation with the solution

$$N_i(t) = \frac{W N_{\gamma}}{\text{rec} n_H} \left(1 - e^{-\text{rec} n_H t} \right); \tag{21}$$

As an order of magnitude estimate, $\text{rec} = 10^{13} \text{ cm}^3 \text{s}^{-1}$ is typical, and $n_H = 10^6 \text{ cm}^{-3}$ might represent a typical cool clump. Thus the exponential term of the solution vanishes after $t \ll 10^7 \text{ s}$, or a few months. Thus an equilibrium condition is quickly met.

Now, a clump is said to be photo-evaporated (i.e., "destroyed") when the total volume has become ionized, with $V_{\text{ioniz}} = V = 4 R^3 = 3$. Setting $N_i = n_H V$ and substituting for W , one obtains the following condition for the survival of a clump:

$$n_H^2 R \geq \frac{3N}{16 r^2_{\text{rec}}} \quad (22)$$

$$\geq 3 \cdot 10^{27} \frac{N}{10^{49} \text{ s}^{-1}} \left(\frac{1000 \text{ AU}}{r} \right)^2 \frac{10^{13} \text{ cm}^3 \text{ s}^{-1}}{r_{\text{rec}}} \text{ cm}^5 \quad (23)$$

The nominal values of $N = 10^{49} \text{ s}^{-1}$ and $r = 1000 \text{ AU}$ were motivated by the application to W 49N (B2 to be discussed in §3 (see also Tab. 1)).

Interestingly, this lower limit can be converted to a minimum free-free optical depth that is required for clump survival. Recall that the clump optical depth along its diameter is $\tau = 2 R$. Noting that $n_i n_e = n_H^2$, and evaluating the opacity for a frequency of $\nu = 10^{10} \text{ Hz}$, the minimum optical depth for clump survival is

$$\tau \geq 1; \quad (24)$$

evaluated for a temperature of $T = 10,000 \text{ K}$. This limit is useful because it effectively truncates the $N(\tau)$ distribution, which as shown in the following section, can have ramifications for the bandwidth over which intermediate power-law segments will exist.

2.4. Parameter Study

In Figure 4 calculations of model SEDs are shown for a range of β values as indicated. Recall that $N/\tau \propto \beta^{-1}$ so that for $\beta < 1$, thicker clumps dominate the population and for $\beta > 1$, thinner clumps dominate the population. In each panel the solid line is the normalized SED with values corresponding to the ordinate at left. Note that for $\beta = 1$, the lower and upper limits to the optical depth distribution are 0.01 and 100, respectively. The dashed line is the local power-law slope (i.e., first derivative of the SED), with ordinate to the right. The dotted line is the variation of the power-law index in normalized frequency (i.e., the second derivative of the SED). Although no separate axis is given for the dotted curve, its value is generally negative because the SEDs are concave down, and zero wherever the SED is linear in the log-log plot of Figure 4.

The turnover from a thick spectrum to one that is thin has a minimum in the curve for the second derivative. Generally, a single minimum indicates a smooth and continuous turnover from a thick to a thin spectrum. However, the case of $\beta = +1$ shows a departure from this trend, displaying two downward peaks, indicating three distinct portions of the spectrum that exhibit a power-law. In fact, the two peaks define a frequency "window" or band for an intermediate power-law with a slope between +2 and 0.11.

Figure 5 shows more SED calculations for a finer grid of β values, focussing on the range of $\beta = 1$ to 2. In this range intermediate power-law segments persist with windows of about 1 dex in frequency. At $\beta = 1$ the slope of the intermediate power-law is high at about 1.6, but with increasing β , the value of β drops. The frequency windows are narrower for $\beta = 1$ and 2. As seen in Figure 4, the SED turnover is smooth and regular for β values outside the range of 1{2. Hence, we come to the interesting conclusion that a rather restricted range of β values are suitable for producing intermediate power-laws of significant bandwidth.

To illustrate better how intermediate power-law segments arise, Figure 6 shows a model SED using a value of $\beta = 1.5$. The solid line is the SED from the clump ensemble. The dotted lines are for contributions

to the net spectrum from clumps of different optical depths (artificially shifted upward for clarity of display). The SEDs of individual clumps show a power-law segment of f^2 at low frequency and one of $f^{-0.11}$ at high frequency, the two joined by a fairly rapid turnover. The different combination of clumps with different optical depths at the crucial frequency ν_0 serves to "spread out" the turnovers of the individual clump SEDs, so as to produce in the net SED a significant power-law segment that has a slope intermediate between +2 and -0.11.

It is crucial to consider how the lower and upper optical depth scales for the clump distribution influence the SED. Figure 7 shows more models of the case $\tau = 1.5$, now with the upper limit t_2 fixed at 100, and the lower limit t_1 varied from 0.0001 to 10 as indicated. As the lower limit t_1 approaches the upper limit value, the bandwidth of the intermediate power-law grows progressively narrower, nearly to disappear in the final panel. This is reasonable, because as t_1 approaches t_2 , the distribution of clump optical depths becomes progressively narrower, eventually to approach a δ -function. Figure 8 shows a similar kind of plot, but now t_1 is fixed at a value of 0.001, and the upper limit t_2 is decreased by factors of 10 from 10,000 down to 0.1. As t_2 approaches t_1 , the intermediate power-law segment again narrows.

Conclusions from varying the upper and lower optical depth limits are as follows. (a) When the ratio $t_2=t_1$ is near unity, the resulting SED is essentially that of a single clump. (b) As the ratio is made large, an intermediate power-law segment can arise for certain values of τ , and large ratios of $t_2=t_1$ maximize the frequency window over which this segment persists. And (c) assuming a significant power-law segment exists, changing the individual values of t_1 and t_2 shifts the power-law segment in frequency. Increasing t_2 shifts the window to higher frequency, whereas decreasing its value results in a shift to lower frequencies.

Next, we use the experience gained from our parameter study to model the spectrum of the HC III region W 49N-B2 which exhibits an observed radio SED characterized by a power-law index of +0.9.

3. APPLICATION TO W 49N-B2

The thermal radio source W 49A, first observed by Westerhout (1958), lies at a distance of 11.4 kpc (Gwinn, Moran, & Reid 1992) and is composed of two main components W 49A-N and W 49A-S which are generally referred to simply as W 49N and W 49S. With high spatial resolution, these two main components resolve into multiple, luminous radio components. Deher et al. (1984) and DePree et al. (2000) resolve W 49N into nine or more very compact and luminous radio-continuum components. Of the nine sources identified by DePree et al. (2000) in W 49N, seven have broad radio recombination lines ($\sim 40 \text{ km s}^{-1}$) and rising spectra in the wavelength range 13 mm to 3 mm. We have selected one of the brightest of these, W 49N-B2, from DePree et al. (2000) to attempt to fit its SED from 13 mm to 3 mm (spectral index of $\alpha = +0.9$). This compact, luminous radio source has a measured radius of 0.007 pc, an rms electron density of $1.3 \times 10^6 \text{ cm}^{-3}$, an emission measure of $2.4 \times 10^6 \text{ pc cm}^{-6}$, and an ionizing photon flux of $2 \times 10^8 \text{ s}^{-1}$, corresponding to an equivalent ZAMS spectral type of O5.5 or hotter (DePree et al. 2000). W 49N-B2 has a shell-like morphology with lower brightness extensions to the NE and SW (see Fig. 2 of DePree et al. 2000). A water maser has also been detected $\sim 1''$ to the north of the W 49N-B sources.

To model the spectrum of W 49N-B2, we also include a 1.4 mm observation from Wilner et al. (2001). At this wavelength the calibration is much more difficult. We have used the radio image appearing in their Figure 1 (ii) to infer a lower limit of 400 mJy at 1.4 mm, that appears as a point with an upwardly directed arrow in the lower panel of Figure 9. Although earlier work suggested a power-law slope of $\alpha = 0.9$ around 7 mm (appearing as the dotted line in the lower panel of Fig. 9), the lower limit of Wilner et al., in conjunction with their discussion of adjacent sources, suggests that the spectrum is becoming optically thin around 2 mm.

Although Figure 9 indicates that a satisfactory match to the shape of the SED can be obtained with

our model for a clumpy medium, it remains for us to determine if we can match the scale of the observed flux. From equation (14) for the parameter F_0 and equation (15) for the definition of the covering factor, one obtains

$$F_0 = \frac{4 k h T_i L^2}{\lambda_0^2 D^2} C \quad (25)$$

We introduce a parameter f as

$$f = \frac{R}{\lambda_0} \frac{\int_0^R N(t) G(t) dt}{\int_0^R N(t) dt} \quad (26)$$

so that the source flux can be re-expressed as

$$F = F_0 f \quad (27)$$

Using values from Table 1 for W 49N-B2, and assuming that $h T_i = 8000 \text{ K}$, we have evaluated F_0 at the wavelength $\lambda_0 = 7 \text{ mm}$, which gives $F_0 = 1080 \text{ m Jy } C$. The observed flux level at 7 mm is $F = 550 \text{ m Jy}$. From Figure 9, we find a value of $\log f = \log \frac{R}{\lambda_0} = 0.92$. Combining these numbers yields a covering factor of $C = 0.15$, which is quite small indicating that shadowing of clumps by other clumps is not a major concern for this source. In other words, foreground clumps are not absorbing emission from rearward clumps.

Indeed, the shadowing effects implied by $C = 15\%$ should be considered an upper limit for the following reason. Our covering factor is defined purely in terms of geometry. If the majority of clumps are optically thin, then the "effective" covering factor may actually be less, since shadowing by thin clumps does not result in much absorption (unless the accumulated column depth of multiple clumps produces a significant optical depth in total). For example, our model is for $\tau = 1.4$ with $t_2 = 1000$ and $t_1 = 0.1$ at $f = 1$ (appearing in the upper panel of Fig. 9). At the wavelength of 7 mm , these upper and lower optical depth limits become approximately 10 and 0.001, respectively. The mean clump optical depth is thus only $\tau = 0.2$, and just 4% of the clumps have optical depths in excess of unity along their diameters. Consequently, the effective covering factor is closer to $4\% = 15\% \times 0.6$. Even at 15%, the shadowing is not severe for W 49N-B2; however, this discussion illustrates how application of this model to other sources may need to take into account optical effects when interpreting geometric covering factors if found to be of order unity or larger.

If the analysis of W 49N-B2 is valid, then information about the optical depth distribution of the clumps has been inferred. Although optical depth is the natural variable to be deduced from observables, the preferred distributions to test against theoretical models are in density and size. Of course, the optical depth distribution that is derived from the data can be related to the density and size properties of the clumps. This is achieved by taking density and size distributions from theoretical considerations and simulations, and transforming them to a distribution in τ . Generally, if the densities and sizes for the clumps individually obey power laws, then the optical depth distribution will also be a power law, since $\tau \propto \rho^2 R$ for uniform clumps. Consequently, our method that is sensitive to the optical depth properties of the clumps can help to constrain models that predict density and size distributions.

4. DISCUSSION

The advantage of using uniform, spherical clumps is that the emission from an individual clump can be derived analytically, and analytic derivations are useful for facilitating insight into a problem. On the

other hand, analytic derivations usually arise from assuming some simplifying conditions. In this case the sphericity of the clumps is a simplification, but unlikely to be important enough to change basic conclusions. Uniformity of the clumps may pose a more severe problem. In reality, inhomogeneities near hot stars are probably cold, neutral, and dense cores with a "skin" of ionized, photo-evaporating, gas. It is these ionized layers (plus any diffuse component existing between the clumps) that produce the observed free-free emission.

At frequencies for which these layers are optically thick, our analysis based on spherical clumps is equivalent because all that matters is the projected area of the clumps. At frequencies for which the layers are entirely thin, our method predicts the same slope for the attenuated spectrum, but overestimates the scale of the emission (by the factor of the ratio of the clump volume relative to the layer volume). But what is the impact of ionized layers for the intermediate power-law segments to SEDs that we have derived here? Qualitatively, the treatment of uniform spherical clumps allows for a greater range of optical depths across the face of the clump than for a layer. That is, if the layers are geometrically thin relative to the clump size, then the layer is nearly plane-parallel, so that $\tau(\nu)$ will be similar across the clump face. This suggests that in the case of ionized layers, the turnover in frequency from the thick +2 slope to the thin 0:1 slope will occur over a narrower bandwidth as compared with uniform clumps. How this affects the power-law segments is not clear. The sharper turnover in the SED of a single clump may lead to better power-law segments (i.e., segments of more nearly constant slope and less curvature) than for uniform clumps; however, these segments may exist over a narrower bandwidth. This topic needs to be investigated quantitatively.

Also needed is an extension of the results derived here to the case when the covering factor exceeds unity. More specifically, the influence of optical depth effects need to be included for the case of clumps that "shadow" other clumps. As pointed out in the application to the W 49N (B2) source, the covering factor defined in this paper is one of geometric cross-section only.

It is possible to predict to some degree the influence of optical depth on the covering factor. Specifically, C will be a function of frequency. At frequencies for which all clumps are thick, the limit of C defined purely in terms of the accumulated cross-section of all clumps is valid, and in this limit C achieves its largest value. However, the SED when all clumps are thick remains a +2 power law. So, when compared to our present treatment that ignores clump shadowing, the SED shape remains the same for the limit that all clumps are thick; only the scale of the emission is overestimated, since the emission from many rearward clumps do not emerge to the observer. In other words the greatest level of emission from a region of size L is $F = 2 B L^2 = D^2$.

At the opposite extreme, the covering factor drops to zero at frequencies in which all the clumps are optically thin (or to be more exact, when the average optical depth through the emitting region of size L is less than unity). In this limit geometric shadowing becomes irrelevant because there is little absorption, and so the results that we have presented remain valid, both in the shape of the SED and the scale. Combining the thin portion, which is unchanged, with the thick portion, for which the flux level is overestimated, it appears that the intermediate power-law segments will prove to be steeper. Whether or not these segments will exhibit greater curvature or not is unclear and must be studied with numerical calculations in the future.

5. SUMMARY AND MAIN CONCLUSIONS

We have used expressions for the radio continuum flux density and optical depth of a single, unresolved, uniform (i.e., temperature and density are constant), spherical clump to calculate the SEDs for an ensemble of many such clumps with a power-law distribution of optical depths. The motivations for this morphology are: (1) the empirical evidence for clumping over a wide range of scale sizes in ionized and neutral atomic and molecular phases of interstellar and circumstellar media; and, (2) the intermediate sloped power-law SEDs observed toward a growing number of H C H II regions. The primary thrust of this investigation was to

determine if a power-law SED with slopes intermediate between the optically thick and thin limits of $\alpha = +2$ and -0.1 (where $F \propto \nu^\alpha$) can be understood as a consequence of emission from a hierarchically clumped medium; and, if so, to investigate under what conditions intermediate sloped SEDs are formed and over how large a frequency interval they may occur.

We have found that it is possible for an ensemble of clumps with a power-law distribution of optical depths to produce power-law SEDs of intermediate slope over a limited bandwidth. The frequency interval over which an intermediate slope holds is controlled by the range of clump optical depths for an appropriate distribution of clumps $N(\tau)$. The greater the range in optical depths, τ_{max} to τ_{min} , the broader the bandwidth over which an intermediate slope persists. The slope of the intermediate SED power-law is determined primarily by the parameter β which specifies the fraction of the nebula that is filled with optically thick clumps at a given frequency. In our models, intermediate power-law slopes only appear for values of β between 1 and 2, however, we have not explored all possible values of parameter space.

We find a good fit to the SED of W 49N-B2 using the measured radio parameters for this source from DePree et al. (2000) for an ensemble of clumps with $\beta = 1.5$. The clump optical depths vary from a maximum of 300 to 0.3 at 7 mm and the mean optical depth at this wavelength is 9.5. The geometric covering factor is $C = 0.15$. The covering factor is small enough to easily produce a low density halo around the dense ionized core of this H C H II region, for which some observational evidence exists.

Power-law SEDs of intermediate slopes result from the additive effect of many individual clumps whose turn-over frequencies occur in sequential order over a limited range in frequency. The primary insight gained from our study of hierarchically clumped nebulae is that the distribution of optical depths of the clump population is solely responsible for determining the continuum shape, with variations in size and temperature of the clumps serving only to modulate the level of the free-free emission. Logical extensions of this work would be to investigate the effects introduced by non-spherical clump morphologies, non-uniform clumps (i.e., variations of temperature and density within clumps), and clump shadowing.

We express thanks to Joe Cassinelli, Ken Gayley, and John Mathis for helpful comments relating to the emission from an ensemble of clumps. We are especially grateful to Stan Kurtz for providing Figure 1, and to David Wilner for comments relating to the 1.4 mm flux density measurement for W 49N-B2. We also express appreciation to Doug Johnstone and Phil Myers for several valuable comments on an early draft of this work. Ignace acknowledges support for this study from an NSF grant (AST-0241493) and Churchillwell acknowledges partial support for this work from NSF grant AST-9986548.

R E F E R E N C E S

- Cox, A. N. (ed.) 2000, *Allen's Astrophysical Quantities*, (New York: Springer-Verlag)
- DePree, C. G., Mehringer, D. M., Goss, W. M. 1997, *ApJ*, 482, 307
- DePree, C. G., Wilner, D. J., Goss, W. M., Welch, W. J., McGath, E. 2000, *ApJ*, 540, 308
- Decher, J. W., Johnston, K. J., Welch, W. J., Walker, R. C. 1984, *ApJ*, 283, 632
- Elmegreen, B. G., Falgarone, E. 1996, *ApJ*, 471, 816
- Faison, M. D., Goss, W. M., Diamond, P. J., Taylor, G. B. 1998, *AJ*, 116, 2916
- Faison, M. D., Goss, W. M. 2001, *AJ*, 121, 2706
- Falgarone, E., Phillips, T. G. 1996, *ApJ*, 472, 191
- Falgarone, E., Panis, J.-F., Heithausen, A., Perault, M., Stutzki, J., Puget, J.-L., Bensch, F. 1998, *A & A*, 331, 669

- Garay, G., Rodriguez, L., Moran, J. M., Churchwell, E. 1993, *ApJ*, 418, 368
- Gaume, R. A. 1994, *Lecture Notes in Physics*, Vol. 439, (eds) T. L. Wilson & K. J. Johnson, Springer Verlag, Berlin, 199
- Gaume, R. A., Goss, W. M., Dickel, R., Wilson, T. L., Johnson, K. 1995, *ApJ*, 438, 776
- Gwinn, C. R., Moran, J. M., Reid, M. J., 1992, *ApJ*, 393, 149
- Hartmann, L., Cassinelli, J. P. 1977, *ApJ*, 215, 155
- Hester, J. J., Scowen, P. A., Sankrit, R., Lauer, T. R., Achar, E. A., et al. 1996, *AJ*, 111, 2349
- Hofner, P., Kurtz, S., Churchwell, E., Walmsley, C. M., Cesaroni, R. 1996, *ApJ*, 460, 359
- Koo, B.-C., Kim, K.-T., Lee, H.-G., Yun, M.-S., Ho, P. T. P. 1996, *ApJ*, 456, 662
- Kurtz, S. E., Watson, A. M., Hofner, P., Ote, B. 1999, *ApJ*, 514, 232
- Kurtz, S. E., Franco, J. 2000, *Rev Mex A A*, 12, 16
- Kurtz, S. E. 2000, *Rev Mex A A*, 9, 169
- Kurtz, S. E. 2002, presentation at the 2002 Workshop on Star Formation, Taiwan
- Lazarian, A., Pogosyan, D. 2000, *ApJ*, 537, 720
- O'Dell, C. R. 2001, *ARA & A*, 39, 99
- O'Dell, C. R., Balick, B., Hajian, A. R., Henny, W. J., Burkert, A. 2002, *A & A*, 123, 3329
- O'Dell, C. R., Balick, B., Hajian, A. R., Henny, W. J., Burkert, A. 2003, *Rev Mex A A*, 15, 29
- Olson, F. M. 1975, *A & A*, 39, 217
- Osterbrock, D. E., 1974, *Astrophysics of Gaseous Nebulae*, (San Francisco: W. H. Freeman & Co.)
- Panagia, N., Felli, M. 1975, *A & A*, 39, 1
- Shepherd, D., Churchwell, E., Goss, W. M. 1995, *ApJ*, 448, 426
- Shepherd, D. S., Watson, A. M., Sargent, A. I., Churchwell, E. 1998, *ApJ*, 507, 861
- Sewilo, M., Churchwell, E., Kurtz, S., Goss, W. M., Hofner, P. 2003, *ApJ*, submitted
- Westerhout, G. 1958, *Bull. Astron. Inst. Netherlands*, 14, 215
- Wilner, D. J., DePree, C. G., Welch, W. J., & Goss, W. M. 2001, *ApJ*, 550, L81
- Wright, A. E., Barlow, M. J. 1975, *MNRAS*, 170, 41

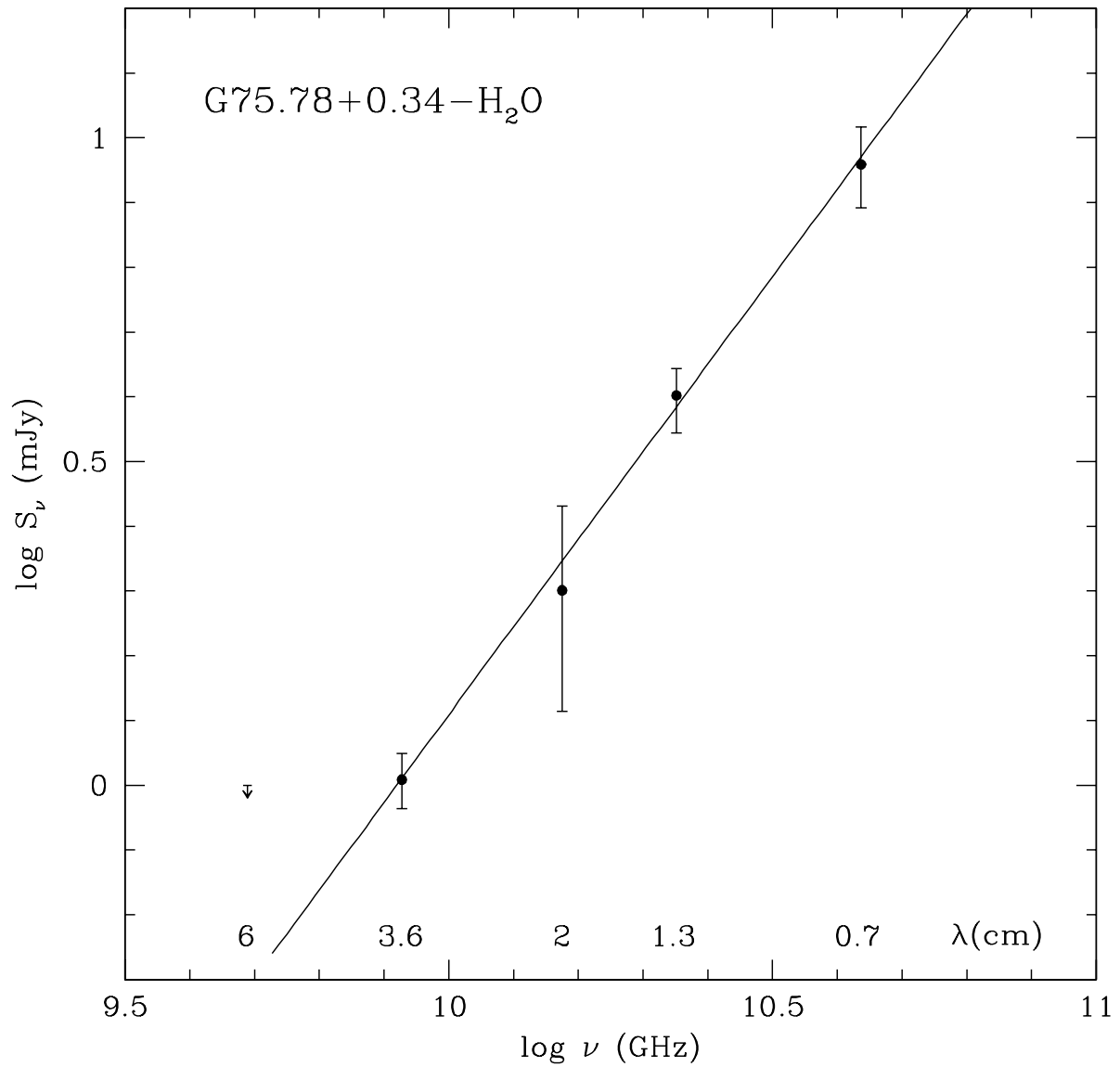


Fig. 1. | The observed spectral energy distribution for G 75:78 + 0:34 H₂O . This object is a good example of an intermediate-sloped power law between 36 and 7 mm . It is not detected at 6 cm , likely because of sensitivity limitations. This figure is courtesy of Stan Kurtz (private communication).

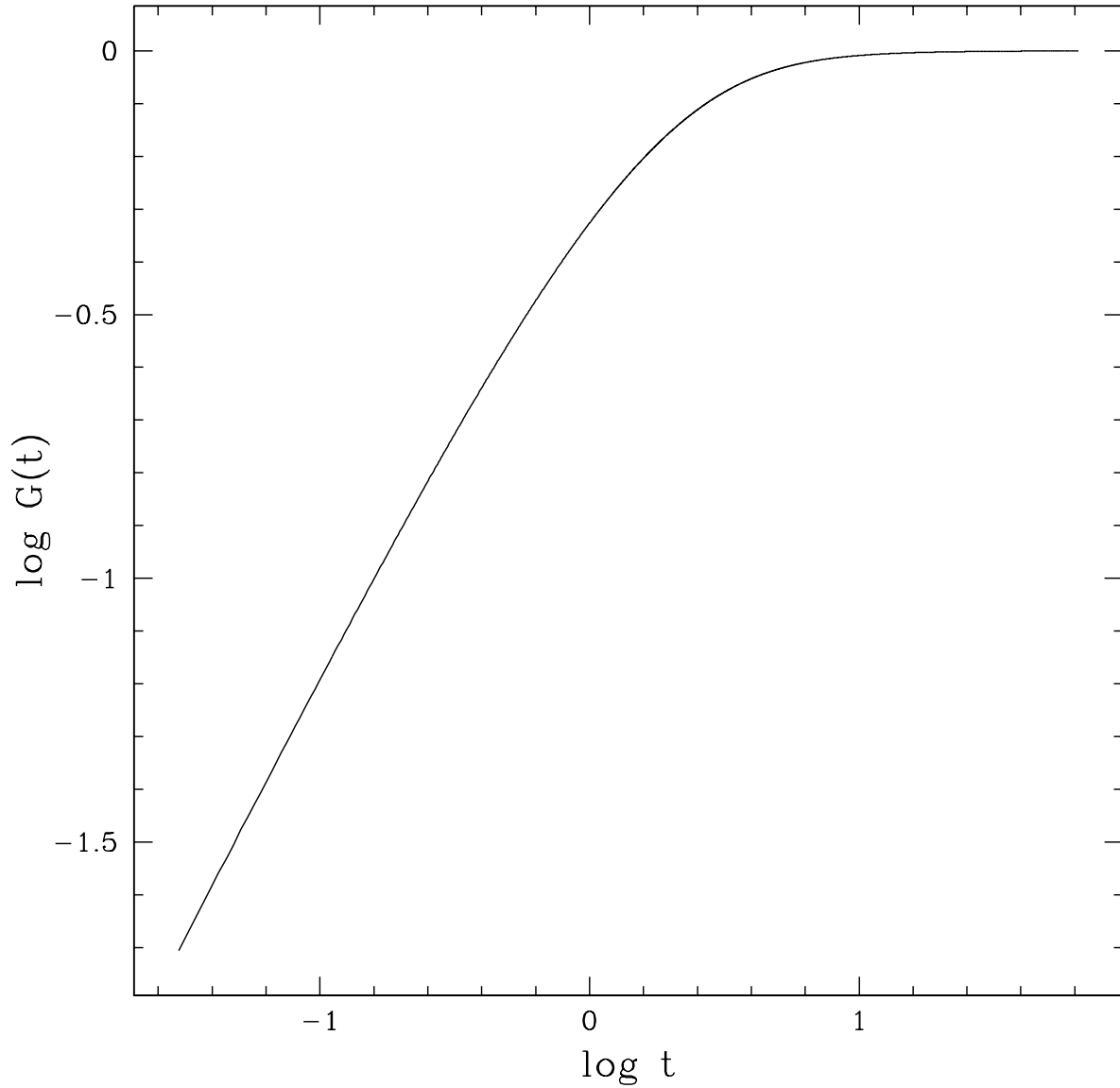


Fig. 2. | A plot of the function $G(t)$. For low optical depths, $G \propto t$, but for optically thick clumps, $G \rightarrow 1$. The function G represents the relative contribution to the flux of emission from individual clumps. Alternatively, it can be viewed as the spectral contribution of a single clump applying the transformation $t/f^2 g$.

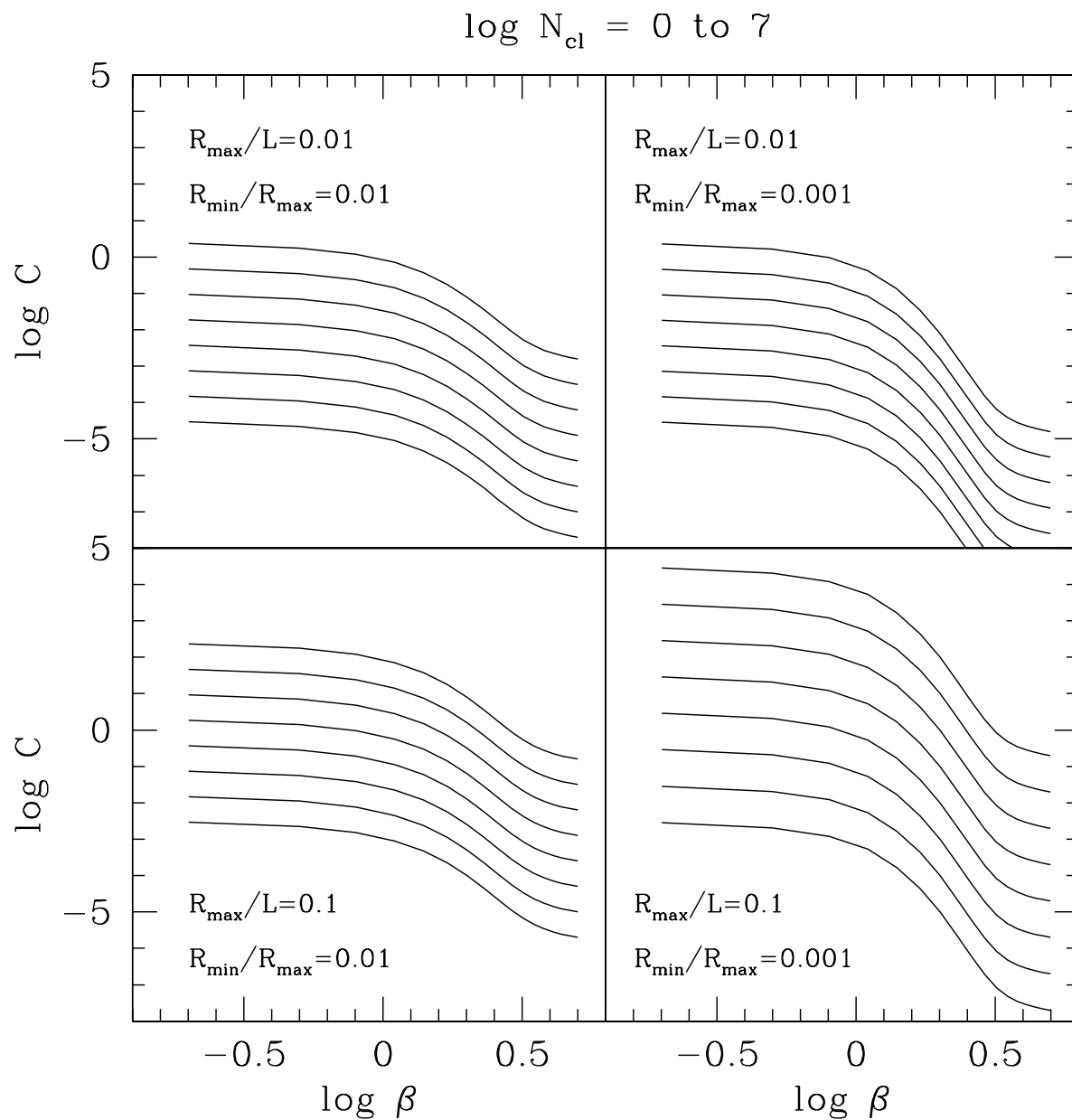


Fig. 3. | A plot of the covering factor C versus the power law exponent β for the distribution of clump sizes. Each curve is for a different number of clumps $\log N_{cl}$ from 0 (always the lowest curve) to 7 (always the highest curve). The four panels are for different values of $R_{max}^2 = L^2$ and $R_{min} = R_{max}$ as labelled.

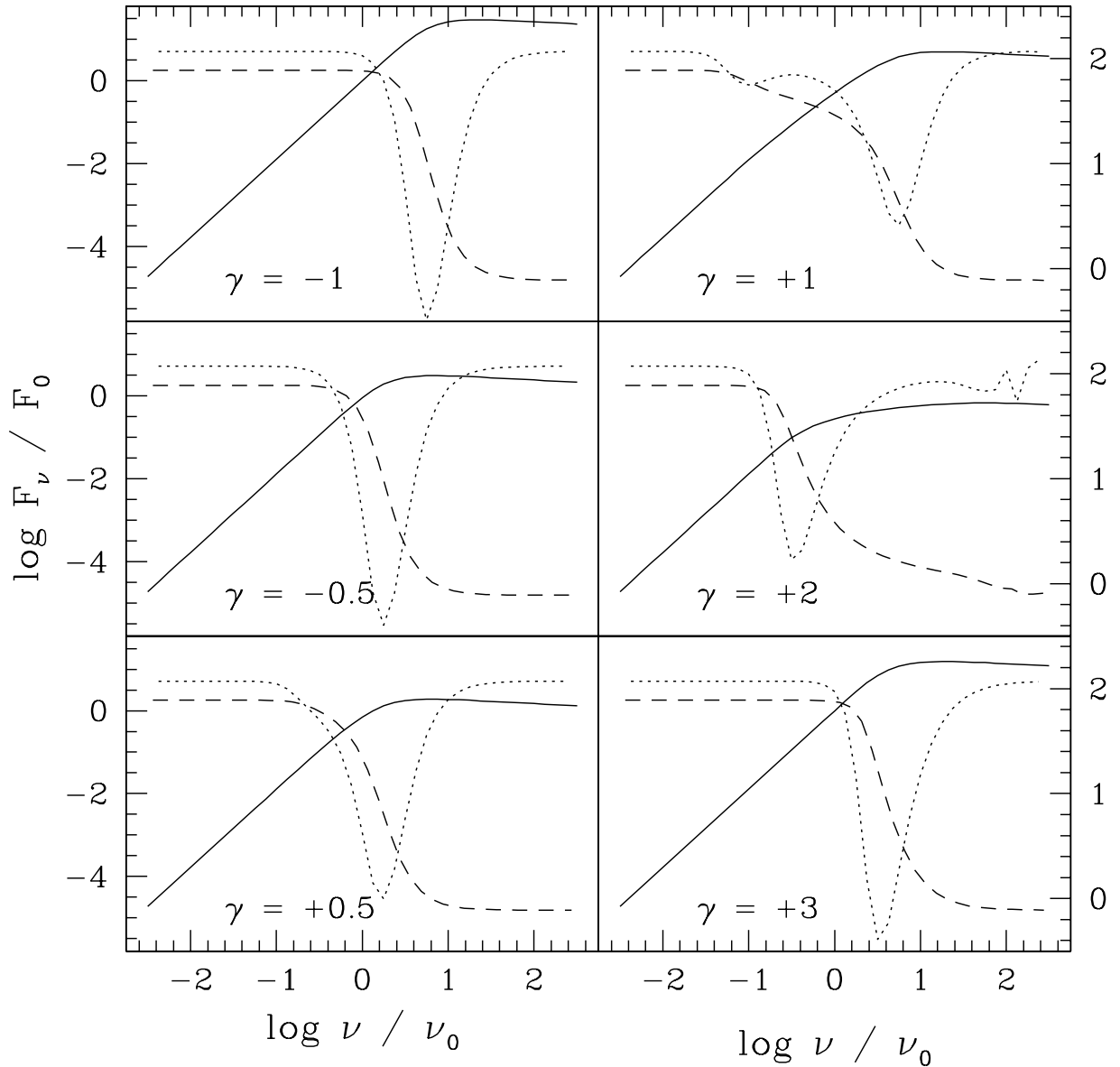


Fig. 4. | A sequence of model SEDs in normalized flux plotted logarithmically against normalized frequency with γ as labelled. The solid line is the SED, with axis at far left. Dashed is the first derivative of the spectrum, with axis at far right. Dotted is the second derivative of the spectrum, which although it has no axis of its own is negative or near zero because the spectral shapes are concave down. Downward peaks in the second derivative curve indicate a transition between power-law slopes in the SED. Note that for the middle right panel, the rapid variations in the first and second derivative curves at far right are numerical artifacts, and occur where the SED happens to be extremely flat. (Also seen in Fig. 5.)

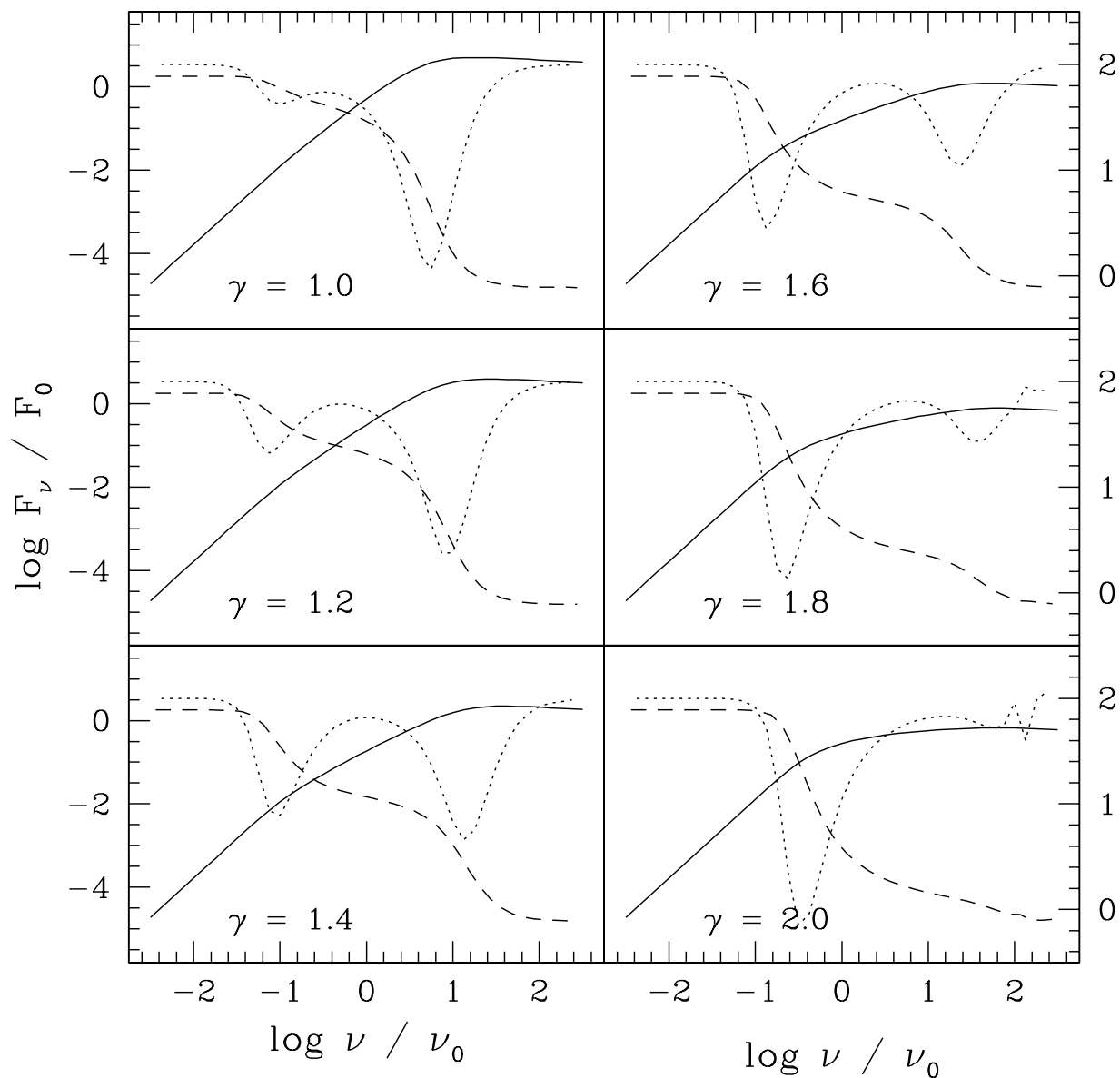


Fig. 5. | A sequence of model SEDs similar to Fig. 4, now for a narrower range of γ values. In the range of $\gamma = 1 - 2$, a power-law segment with slope intermediate of +2 and 0:11 exists over a significant bandwidth. This "window" is demarcated by the two downward peaks in the second-derivative curve (dotted).

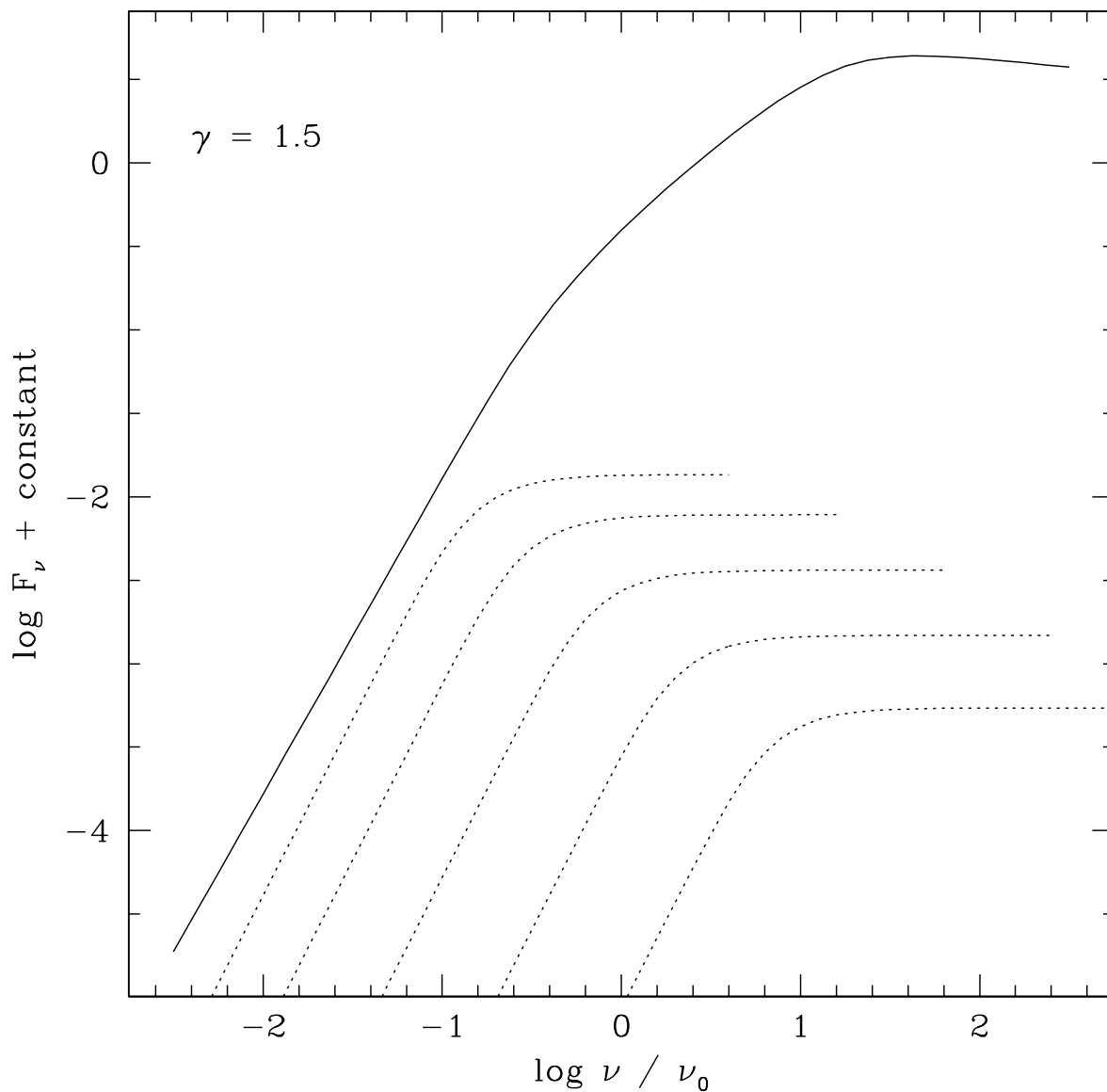


Fig. 6. | An illustration of how intermediate power-laws result. The solid line is an SED for $\gamma = 1.5$. The dotted lines are contributions (with an arbitrary vertical shift) from subgroups of clumps that have different optical depths at $\nu = \nu_0$. Although all the dotted curves are similar, the turnover from a thick spectrum to one that is thin is shifted laterally from curve to the next, leading in the superposition to an intermediate power-law slope.

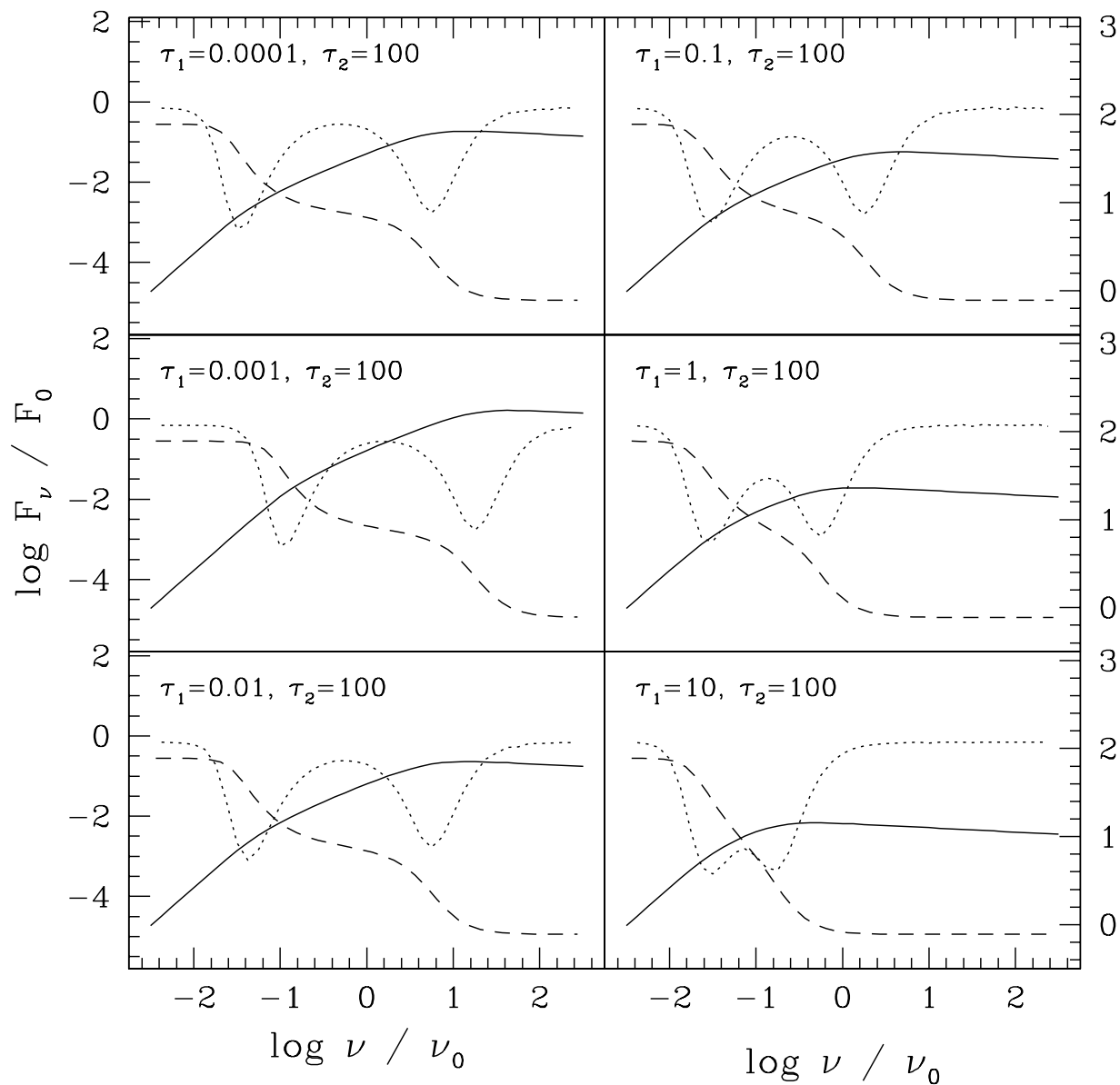


Fig. 7. | Another sequence of model SEDs, similar to Fig. 4, now with $\beta = 1.5$ fixed. For the $N(t)$ distribution, the upper limit t_2 is fixed at 100, and the lower limit t_1 is allowed to vary as indicated. As the lower limit is increased, the bandwidth for the intermediate power-law segment narrows and shifts to lower frequency. The spectrum also drops in relative brightness.

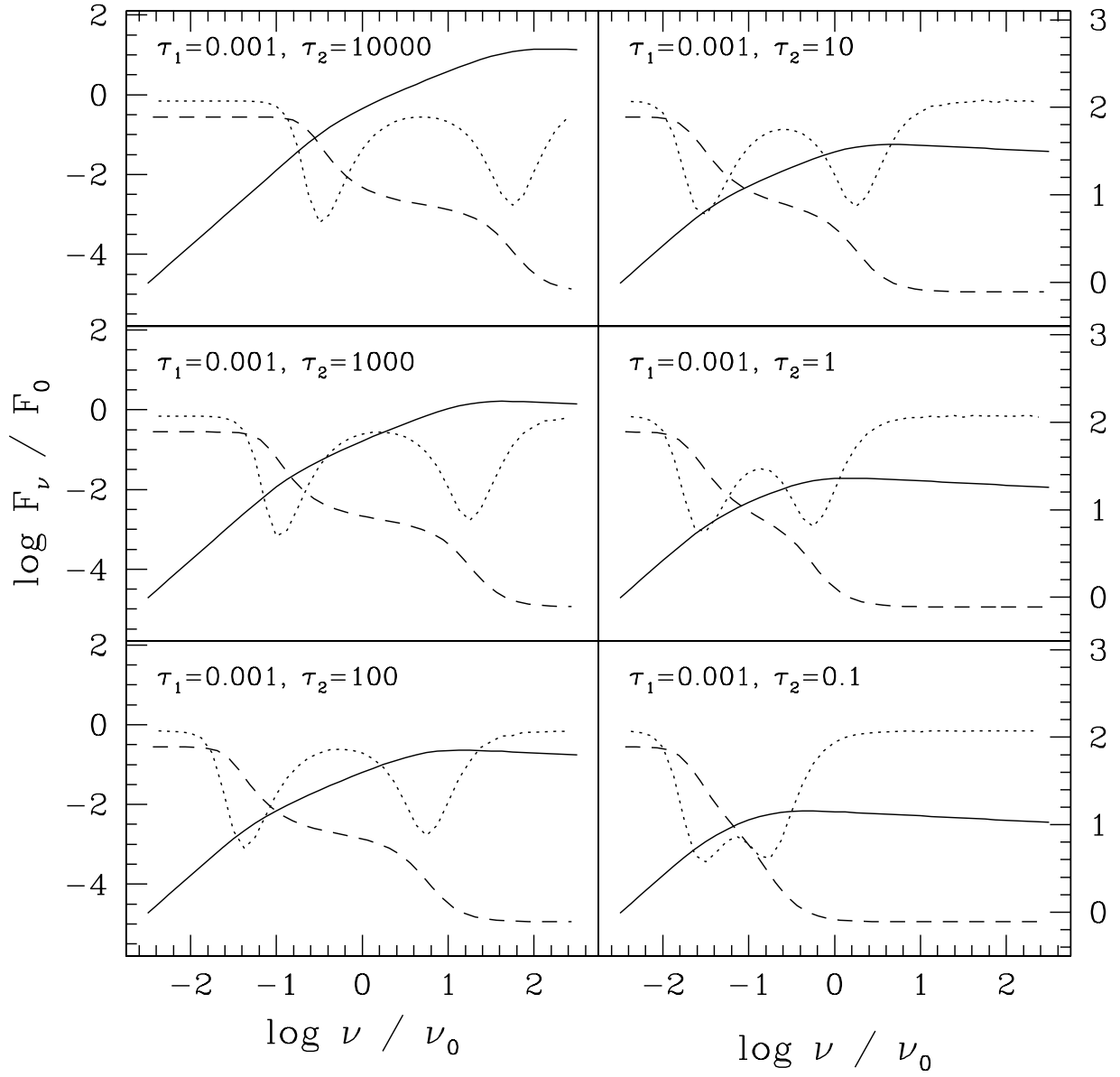


Fig. 8. Similar to the preceding figure, but now with $\tau_1 = 0.001$ fixed and τ_2 varied from 10000 down to 0.1 as indicated. Essentially identical behavior is observed for the change in the SED properties.

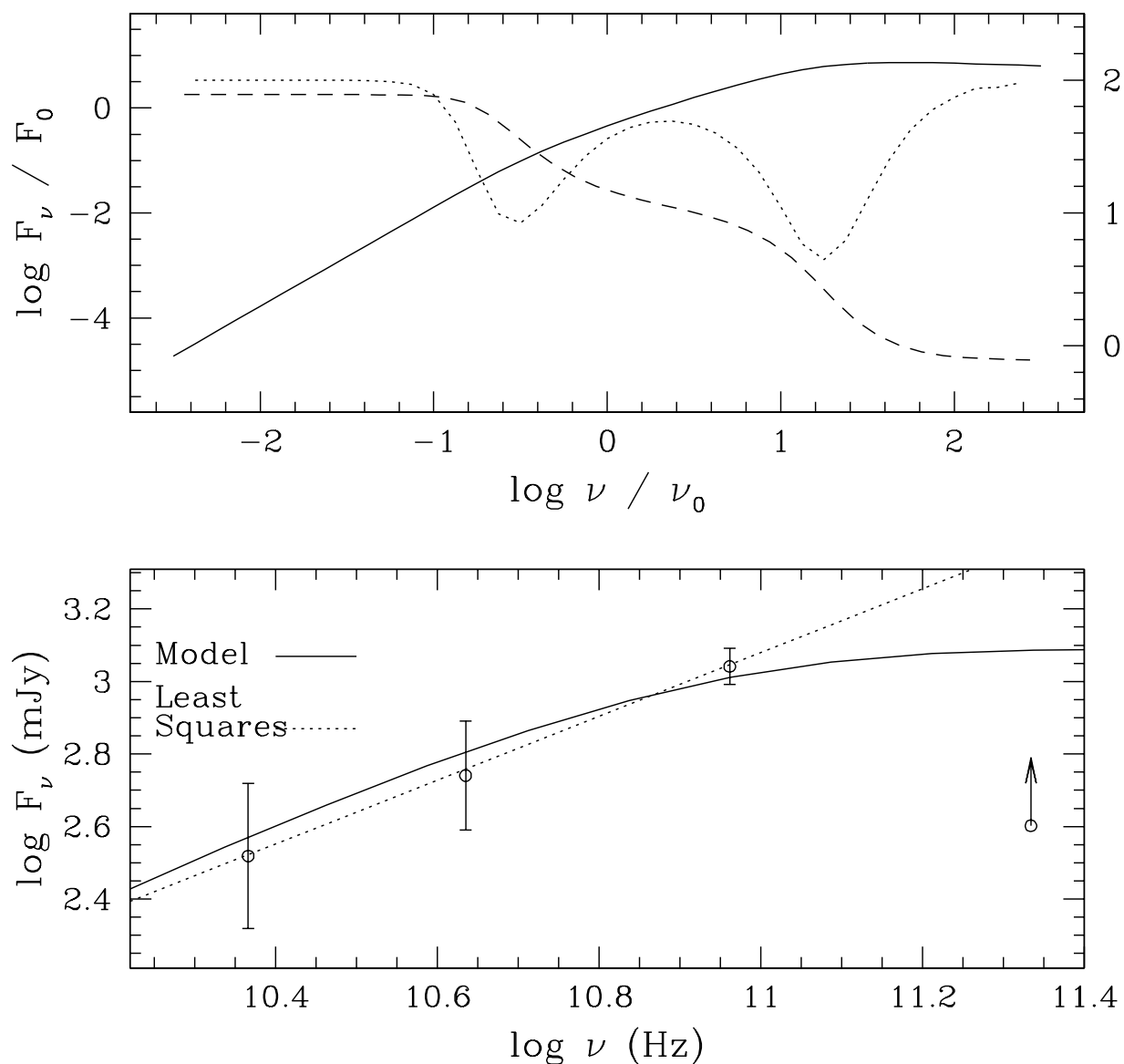


Fig. 9. Top: The case of $\tau = 1.4$ yields an intermediate power-law SED of slope $+1.0$ over a significant frequency bandwidth, bounded to the right by a turnover to an optically thin spectrum, and to left by an optically thick one. Bottom: Three flux density points measured for the source W 49N (B2), plus a fourth point at right that is a lower limit (from Wilner et al. 2001). The dotted line is a power-law fit to the three data points at left and has a slope of $\tau = +0.88$. The solid line is the model calculation from the upper panel, with F_0 and ν_0 chosen to provide for a turnover to an optically thin spectrum suggested by the lower limit at far right (also see Tab. 1).

Table 1: Properties of W 49N (B2)^a

Parameter	Value
RA (J2000)	19h 10m 13.143s
DEC (J2000)	+ 09 06' 12.52"
d	11.4 kpc
F (1.4 mm)	400 m Jy
F (3.3 mm)	1100 m Jy
F (7 mm)	550 m Jy
F (13 mm)	330 m Jy
SED Slope	+ 0.9
$\ln_e i$	$1.3 \cdot 10^6 \text{ cm}^{-3}$
EM	$2.4 \cdot 10^{40} \text{ pc cm}^{-6}$
N ₊	$2 \cdot 10^{49} \text{ photons s}^{-1}$
L	0.007 pc

^a See De Pree et al. (2000) for errors on all quantities.